A Novel Class of Anticancer Compounds Targets the Actin Cytoskeleton in Tumor Cells

Justine R. Stehn[1], Nikolas K. Haass[3,4,7], Teresa Bonello[1], Melissa Desouza[1], Gregg Kottyan[10], Herbert Treutlein[8], Jun Zeng[8], Paula R.B.B. Nascimento[3], Vanessa B. Sequeira[1], Tanya L. Butler[5], Munif Allanson[2], Thomas Fath[1], Timothy A. Hill[6], Adam McCluskey[6], Galina Schevzov[1], Stephen J. Palmer[1], Edna C. Hardeman[1], David Winlaw[5], Vivienne E. Reeve[2], Ian Dixon[9], Wolfgang Weninger[3,4], Timothy P. Cripe[10], and Peter W. Gunning[1]

Abstract

The actin cytoskeleton is a potentially vulnerable property of cancer cells, yet chemotherapeutic targeting attempts have been hampered by unacceptable toxicity. In this study, we have shown that it is possible to disrupt specific actin filament populations by targeting isoforms of tropomyosin, a core component of actin filaments, that are selectively upregulated in cancers. A novel class of anti-tropomyosin compounds has been developed that preferentially disrupts the actin cytoskeleton of tumor cells, impairing both tumor cell motility and viability. Our lead compound, TR100, is effective *in vitro* and *in vivo* in reducing tumor cell growth in neuroblastoma and melanoma models. Importantly, TR100 shows no adverse impact on cardiac structure and function, which is the major side effect of current anti-actin drugs. This proof-of-principle study shows that it is possible to target specific actin filament populations fundamental to tumor cell viability based on their tropomyosin isoform composition. This improvement in specificity provides a pathway to the development of a novel class of anti-actin compounds for the potential treatment of a wide variety of cancers. *Cancer Res; 73(16); 5169–82. ©2013 AACR.*

Introduction

The idea of targeting the actin cytoskeleton is not new, given its role in cellular transformation and biologic processes such as cell division and cell migration (1–4). It is therefore surprising that there are still no anti-actin compounds used in current chemotherapy (5). The primary reason for this is the inability of existing anti-actin agents to discriminate between the actin cytoskeleton of tumor cells and the actin filaments of the muscle sarcomere. Although actin-targeting drugs such as cytochalasin D and jasplakinolide have shown great promise as antiproliferative agents *in vitro* (6, 7), neither has made it through to preclinical trials due to universal toxicity (8). This has led to the development of agents that target actin regulatory proteins, which are more specifically expressed in the specialized actin cytoskeleton of tumor cells (5).

The mammalian tropomyosins are a family of more than 40 coiled–coil proteins that are an integral component of actin filaments (9). There is mounting evidence from systems as diverse as yeast and mammals that individual tropomyosin dimers form largely homopolymers along the length of actin filaments and regulate the functional capacity of the filament in an isoform-specific manner (10–15). This specificity of tropomyosin isoform composition provides an opportunity to target distinct actin filament populations both within a given cell type and between cell types (9, 16).

We have developed a novel class of anti-tropomyosin (anti-Tm) compounds, which preferentially target cytoskeletal (non-muscle) tropomyosin-containing filaments in cancer cells. The lead compound, TR100, is effective against a panel of neural crest-derived tumor cell lines in both two-dimensional (2D) and three-dimensional (3D) cultures with minimal impact on the contractile properties of isolated rat adult cardiomyocytes (ACM). Using melanoma and neuroblastoma mouse xenograft models, we have also shown that TR100 is effective in reducing tumor cell growth *in vivo* without compromising cardiac function. Showing that it is possible to selectively target actin filaments required for tumor cell survival leads the way to

Authors' Affiliations: [1]School of Medical Sciences, University of New South Wales; [2]Faculty of Veterinary Science, University of Sydney, Sydney; [3]Centenary Institute, Newtown; [4]Discipline of Dermatology, University of Sydney, Camperdown; [5]Kids Heart Research, The Children's Hospital at Westmead, Westmead; [6]Chemistry, School of Environmental & Life Sciences, University of Newcastle, Callaghan, New South Wales; [7]The University of Queensland Diamantina Institute, Translational Research Institute, Woolloongabba, Queensland; [8]Qubist Molecular Design Pty Ltd and Monash Institute of Pharmaceutical Sciences, Monash University, Parkville; [9]Genscreen Pty Ltd, Melbourne, Victoria, Australia; and [10]Division of Oncology, Cincinnati Children's Hospital Medical Center and the University of Cincinnati, Cincinnati, Ohio.

Note: Supplementary data for this article are available at Cancer Research Online (http://cancerres.aacrjournals.org/).

Current address for T.A. Hill: Division of Chemistry and Structural Biology, Institute for Molecular Bioscience, The University of Queensland, Brisbane, QLD, 4072, Australia; and current address for T.P. Cripe: Division of Hematology/Oncology/BMT, Nationwide Children's Hospital, Columbus, OH.

Corresponding Author: Peter W. Gunning, Oncology Research Unit, University of New South Wales, Room 229, Wallace Wurth East (C27), Sydney, NSW 2052, Australia. Phone 61-2-9385-2471; Fax: 61-2-9385-0022; E-mail: p.gunning@unsw.edu.au

doi: 10.1158/0008-5472.CAN-12-4501

developing compounds with improved specificity over existing anti-actin compounds. Therefore, therapeutics based on this novel class of anti-tropomyosin compounds would have the potential to treat a wide variety of cancers beyond neuroblastoma and melanoma.

Materials and Methods

Cells and cell culture

Mouse embryonic fibroblasts (MEF) were isolated and cultured as previously described (17). Melanocytes were isolated from 3 independent donors and cultured as previously described (18). SKN-AS, SKN-SH, SKN-Be2C, IMR-32, SH-EP, B16/F10, and SK-MEL-28 cell lines were purchased from American Type Culture Collection and maintained in Dulbecco's Modified Eagle Medium (DMEM) and 10% (volume for volume; v/v) FBS or Eagle's Minimum Essential Medium (EMEM) and 10% (v/v) FBS. The human melanoma cell lines C8161, 451Lu, WM164, WM35, WM793, and 1205Lu were grown as described (19, 20). Pediatric tumor cell lines STS26T, S462, S462-TY, ST88-14, T265, CMTRL-100, A673, and CRL-11226 were maintained in DMEM with 10% (v/v) FBS and 1% (v/v) penicillin/streptomycin. All other lines were maintained in RPMI with 10% (v/v) FBS and 1% (v/v) penicillin/streptomycin. The identity of all nonprimary lines were confirmed by short tandem repeat fingerprinting and were tested within a few passages of initial description or authentification.

DNA and RNA transfection

MEFs were transfected with either pEYFP-C1/Tm5NM1 or pEYFP-C1/Tm5NM5 constructs using the Amaxa nucleofector apparatus (program A-023) and MEF nucleofector kit 1 (Lonza) according to the manufacturer's instructions. For siRNA transfections, SH-EP cells were transiently transfected with nonsilencing control, Tm5NM1/2 and Tm4 siRNA (Qiagen), as previously described (13, 21, 22).

Generation of stable NIH 3T3 fibroblast cell lines

NIH3T3 cells were grown to 50% confluency in a 6-well plate and then transfected with 3.75 μg per well Tm5NM1 tagged with mCherry or αfastTm tagged with yellow fluorescent protein (YFP) using lipofectamine LTX + PLUS reagent (Invitrogen). Cells were cultured in medium supplemented with 800 μg/mL geneticin (Invitrogen), and clones were selected manually with a pipette 14 days later. Once stably transfected cells were established, cells were maintained in culture medium containing 400 μg/mL geneticin.

Live imaging

SKN-Be2C and ACMs. Cells (2×10^4) and freshly isolated cardiomyocytes were plated onto glass 35 mm glass bottom microwell dishes (MatTek Cultureware). Control or drug-treated cells were imaged every 2 minutes for 30 to 60 minutes from randomly set stage positions on an Olympus IX81 microscope equipped with an environmental chamber heated to 37°C. Images and movies were analyzed and processed using ImageJ software.

Stable NIH3T3 fibroblasts. Cells were plated (8×10^3 cells/quadrant) onto a HiQ4 chambered dish (Ibidi) and treated with dimethyl sulfoxide (DMSO) control or 2 μmol/L TR100 24 hours later. Random regions of interest were imaged every 5 minutes for 24 hours following drug treatment using the Nikon Biostation microscope equipped with a cell incubator regulating temperature and CO_2 levels.

Western blotting

Tropomyosin expression profiles were analyzed via SDS-PAGE as described previously (17). High-molecular weight (HMW) tropomyosins, Tm2, Tm3, Tm6, and Tm1, were assessed using α/9d (17) or 311 (Sigma) and low-molecular weight Tm5NM1/2 and Tm4 using the γ/9d and δ/9d antibodies, respectively (17). Sarcomeric tropomyosins were assessed using the CH1 antibody (Sigma), which recognizes exon 1a of all muscle tropomyosins. Cleaved PARP antibody was purchased from AbCam, α-tubulin and C4 actin antibodies were purchased from Sigma. Western blot analyses were scanned on a Biorad Gel doc imaging system and quantified using ImageJ software.

Modeling

Modeling was done by Qubist Molecular Design Pty Ltd. For detailed modeling information see Supplementary Materials and Methods.

Microfilament disruption assay

Cells were seeded (5×10^3/well) into 8-well chamber slides (NUNC) and treated with 10 μmol/L TR100 for 0 to 8 hours or with 0 to 10 μmol/L TR100 for 24 hours using DMSO as vehicle control. Actin was visualized with Alexa 555 conjugated phalloidin (Molecular probes), and Tm5NM1/2 was visualized with γ\9d (17) followed by anti-mouse Alexa 488 or Alexa 555 secondary antibody (Molecular Probes). Random fields were imaged using an Olympus IX81 microscope. Cells ($n \geq 50$) were scored on the basis of positive filament staining from $n = 3$ independent experiments.

Immunofluorescent imaging

Cells were seeded and immunostained as previously described (17). Cells ($n \geq 100$) were scored from $n = 3$ independent experiments.

Cytotoxic compounds

The anti-tropomyosin compound TR100 was designed and synthesized by T.A. Hill and A. McCluskey. Cytochalasin D was purchased from Sigma Aldrich. Compounds were solubilized in DMSO to give stock concentrations of 50 mmol/L (TR100) and 4 mmol/L (cytochalasin D).

Biochemical fractionation of globular and filamentous actin

The ratio of globular (G-) to filamentous (F-) actin was determined using the G/F-actin assay kit (BK037) according to manufacture's instructions (Cytoskeleton Inc.,). Briefly, SH-EP or MEF cells, seeded at 2.0×10^5 cells/10 cm plate, were treated with TR100 for 24 hours. Cells were harvested in F-actin stabilization buffer (LAS2) and centrifuged at 2,000 rpm for 5 minutes to remove unbroken cells. Lysates were centrifuged at 100,000 × *g* for 1 hour at 37°C. Pellets were resuspended in

equal volumes of F-actin depolymerization solution (urea) and vortexed intermittently over 1 hour at 4°C. Equivalent volumes of supernatant and pellet were resolved by SDS-PAGE and subjected to Western blot analysis, using the C4 antibody to probe for total actin.

Pyrene–actin depolymerization assay

Rates of actin depolymerization were determined from the change in pyrene–actin fluorescence (excitation 365 nm, emission 407 nm) measured using a Spectra Max M3 plate reader (Molecular Devices). Tm5NM1 (10 μmol/L) was preincubated with TR100 for 10 minutes, before mixing with F-actin (6 μmol/L, 35% pyrene labeled). Depolymerization was initiated by diluting filaments 12-fold with F-actin buffer [100 mmol/L NaCl, 10 mmol/L Tris-HCl, pH 7.0, 2 mmol/L $MgCl_2$, 1 mmol/L EGTA, 0.2 mmol/L ATP, 0.5 mmol/L dithiothreitol (DTT)], and fluorescence was recorded every 30 seconds over 2 hours. Initial rates of depolymerization (V_0) were determined from the first 600 seconds of fluorescence, fitted to a linear regression model.

Cell viability assays

Cells (1×10^3/well) were plated (96-well) and treated (48 hour) with anti-tropomyosin drug and viability measured using 3-(4,5-dimethylthiazol-2-yl)-2,5-diphenylterazolium bromide MTT. Cell viability was normalized to control (vehicle alone) and dose–response curves, and half maximal effective concentration (EC_{50}) values were determined using Graph Pad Prism 5 (nonlinear regression sigmoidal dose–response variable slope).

Clonogenic assays

siRNA-transfected cells were seeded 48 hours posttransfection into 6-well plates (250 cells/well). Media was changed every 3 days for 7 to 10 days until visible colonies formed. Colonies were fixed and stained and the surviving fraction was determined as previously described (23).

Melanoma spheroid cultures

Melanoma spheroids were prepared using the liquid overlay method as described (24, 25). Spheroids were treated with TR100 for 72 hours at the concentrations indicated. Spheroids were washed in PBS before live-dead staining with 4 mmol/L calcein-AM and 0.5 $\mu g.mL^{-1}$ 4′, 6-diamidino-2-phenylindole (DAPI; Invitrogen) for 1 hour at 37°C. Images were then taken using a Leica SP5 inverted confocal microscope.

Cell migration assays

SH-EP cells were grown in a 6-well plate until confluent. Monolayer was scraped with a p200 pipette tip and cells treated with sublethal concentrations of TR100 (2.5 μmol/L) or cytochalasin D (20 nmol/L). Images were acquired at 0 and 15 hours, and the area of the wound was measured using ImageJ software.

Long-term hippocampal cultures

Low-density long-term hippocampal neurons were prepared as previously described (26). After 19 days, *in vitro* cells were treated with 0 or 2 μmol/L TR100 for 48 hours. Neurons were fixed and cells were costained for synaptophysin as a presynaptic marker and fluorophore-tagged phalloidin (postsynaptic marker) to visualize synaptic connection.

Flow cytometric analysis

SK-MEL-28 cells were seeded (1.5×10^5 cells/well) in 6-well plates and treated with TR100 (0–10 μmol/L) for 2 to 24 hours. Adherent and floating cells were harvested and pelleted by centrifugation (~300 g/5 minutes) at room temperature.

DNA fragmentation by propidium iodide staining. Cells were fixed and permeabilized with 500 μL of cold (−20°C) 70% (v/v) ethanol and treated with propidium iodide (50 μg/mL; Sigma) and RNase A (2 μg/mL; Sigma).

Mitochondrial membrane potential change (Δψm) by TMRE staining. Recovered cells were resuspended in phenol red-free DMEM and stained with 100 nmol/L tetramethylrhodamine 9-ethylester (TMRE; (Molecular Probes) for 15 to 20 minutes as per manufacturer's instructions. Cell cycle and TMRE fluorescence was measured using a FACS Calibur (Becton Dickson) and quantitated using FlowJo software.

Isolation and functional analysis of adult rat cardiomyocytes

ACMs isolation and functional analysis were conducted as previously described (27). Briefly, unloaded cells were paced (MyoPacer, IonOptix) to contract at a frequency of 1 Hz, whereas sarcomere length was recorded following a baseline, drug treatment, and recovery phase.

Animal studies

For detailed methods, see Supplementary Materials and Methods.

Histology and heart hypertrophy measurements

B16/F10 animal hearts ($n = 15$ from each condition) were fixed in 10% (v/v) neutral buffered formalin for 24 hours. Transverse sections of the hearts were embedded in paraffin and serial sections (5 μmol/L), Massons Trichrome stained, and assessed (blinded) for the presence of necrosis and/or fibrosis. Intraventricular septum thickness (IVS) was measured (μmol/L) for control and 30 mg/kg^{-1} TR100-treated animals.

Troponin I measurements

Mice were bled via the retro orbital sinus, and levels of circulating troponin I were detected using a mouse cardiac-specific troponin I enzyme immunoassay (CTnI Elisa-MP BioMedical).

Liver function tests

Control- and TR100-treated 1205Lu xenograft mice were euthanized by CO_2 asphyxiation, and peripheral blood was collected by cardiac puncture. Blood was collected in EDTA-coated tubes (MiniCollect; GBO) before centrifugation for 5 minutes at $1000 \times g$ to separate plasma. Plasma samples were a stored at −80°C. Levels of aspartate aminotransferase (AST) and alanine aminotransferase (ALT) alkaline phosphatase

(ALP) and total bilirubin were determined using a Konelab 20 XTi Clinical Chemistry Analyzer (Thermo Scientific).

Statistical analysis

All data were expressed as mean ± SEM for $n \geq 3$ experiments. P values were calculated using a two-tailed Student t test with unequal variance. $P < 0.05$ was considered statistically significant. *, $P < 0.05$; **, $P < 0.01$; ***, $P < 0.001$; ‡, not significant NS.

Results

Tumorigenic cells have an increased reliance on LMW tropomyosins

The predominant cytoskeletal tropomyosin isoforms in primary tumors and tumor cell lines are the HMW tropomyosins, Tm1 (*TPM2* gene), Tm2, Tm3, and Tm6 (*TPM1* gene), and the LMW tropomyosins, Tm5NM1/2 (*TPM3* gene) and Tm4 (*TPM4* gene; Fig. 1A; ref. 16). We quantified changes in

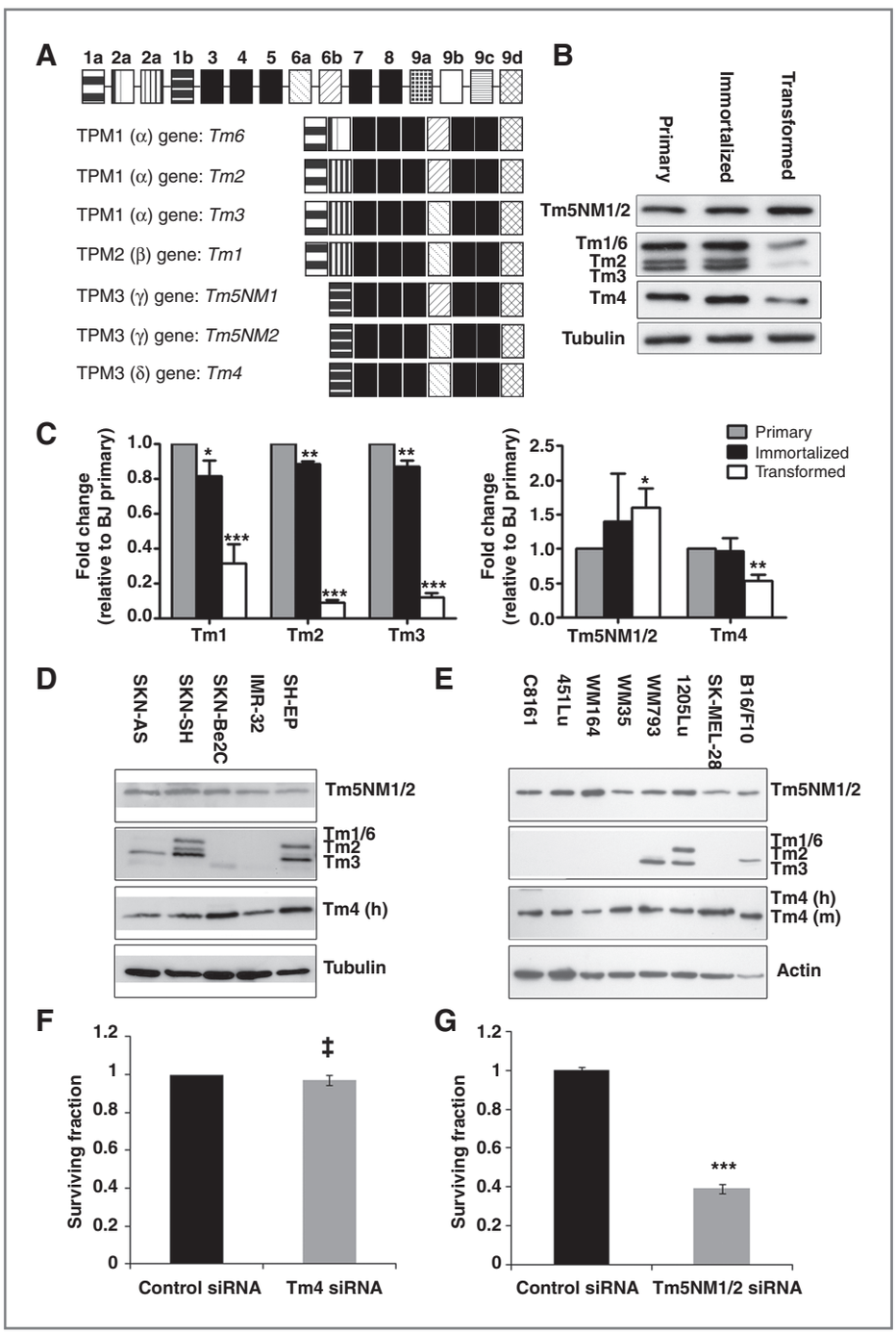

Figure 1. LMW cytoskeletal Tm5NM1/2 is an integral component of the specialized actin cytoskeleton of tumor cells. A, splice variant alignment of the tropomyosin isoforms predicted to be expressed in tumor cells. Western blot analysis (B) and quantitation (C) of expression levels of LMW Tm5NM1/2, HMW tropomyosins 1, 2, 3, and 6, and LMW Tm4 in primary (gray bars), immortalized (black bars) and transformed (white bars) BJ fibroblasts. Tropomyosin expression profile for a panel of neuroblastoma (D) and melanoma (E) tumor cell lines showing levels of LMW Tm5NM1, HMW tropomyosins 1, 2, 3, and 6, and human (h) and mouse (m) variant of LMW Tm4. Colony-forming assay of SH-EP cells transfected with nonsilencing (black bar) or silencing (silver bar) Tm4 (F) or Tm5NM1 (G) siRNA. Data points in F and G represent the average of $n = 3 \pm$ SEM. *, $P < 0.05$; **, $P < 0.01$; ***, $P < 0.001$. ‡, not significant.

tropomyosin levels, which accompany cellular transformation in primary, immortalized, and transformed BJ fibroblasts (28). Cellular immortalization and transformation of the primary BJ fibroblasts lead to significant decreases in HMW tropomyosins (Tm2, Tm3, and Tm1) and LMW tropomyosin (Tm4) expression (Fig. 1B and C). A significant increase in the level of LMW Tm5NM1/2 was observed (Fig. 1B and C) indicating that Tm5NM1/2 is the predominant tropomyosin isoform of these transformed cells.

Endogenous tropomyosin levels were analyzed in a panel of neuroblastoma and melanoma cell lines. Representative neuroblastoma cell lines included both nonmalignant (SH-EP, SKN-SH, and SKN-AS) and malignant (IMR-32 and SKN-Be2C) tumor cells (29). Although there was variation in the levels of expression of the HMW tropomyosins (Tm6, Tm1, Tm2, and Tm3), all cell lines expressed the LMW-Tm4 and Tm5NM1/2 (Fig. 1D). A similar trend was observed for the melanoma cell lines. The panel of melanoma cell lines included 6 human (C8161, 451Lu, WM164, WM35, WM793, 1205Lu, and SK-MEL-28) and one mouse (B16/F10) melanoma cell line. The human melanoma cell lines were derived from primary (WM35 and WM793), lymph node metastatic (WM164), and distant metastatic (C8161, 451Lu, and 1205Lu) disease (http://www.wistar.org/lab/meenhard-herlyn-dvm-dsc/page/melanoma-cell-lines-0). Only WM793, 1205Lu, and B16/F10 expressed HMW tropomyosins. In contrast, all melanoma cell lines expressed the LMW Tm4 and Tm5NM1/2 (Fig. 1E).

Tm5NM1/2 promotes tumor cell growth and survival

The role of the LMW Tm5NM1/2 and Tm4 in tumor cell growth was tested in SH-EP neuroblastoma cells using siRNA knockdown. A specific reduction was observed in Tm5NM1/2 and Tm4 siRNA protein expression levels (>50%; Supplementary Fig. S1A and S1C) with no corresponding compensation from the other tropomyosin isoforms (Supplementary Fig. S1B and S1D). Knockdown of Tm4 in SH-EP neuroblastoma cells did not impact cell survival in a clonogenic assay (Fig. 1F), whereas knockdown of Tm5NM1/2 resulted in a significant decrease in cell survival (Fig. 1G). These data suggest that Tm5NM1/2 containing actin filaments are required for tumor cell survival, and targeting these specific actin filaments compromises tumor cell growth.

Tm5NM1/2 as a therapeutic target

In this novel approach, we have designed a series of compounds against the cytoskeletal Tm5NM1/2. To discriminate between functionally distinct actin filament populations, we took advantage of the C-terminus sequence divergence between the cytoskeletal Tm5NM1/2 and the muscle tropomyosin (αTmfast; Fig. 2A). Using homology modeling and the Molsoft CICM's pocketfinder software, we identified a number of potential compound-binding pockets in both proteins (Fig. 2B and C). Binding pockets unique to the C-terminus of Tm5NM1 (red pocket highlighted in Fig. 2C) were then used to screen a chemical library from which we identified the lead anti-tropomyosin compound, TR100 (Fig. 2D). *In silico* modeling shows the predicted interaction of TR100 to the C-terminus (9d exon) of Tm5NM1 (Fig. 2D).

One difficulty in screening for compounds, which target a coiled–coil protein such as tropomyosin, is that it is a structural protein rather than an enzyme, so developing a high-throughput assay with an appropriate readout of "activity" is challenging. To screen for anti-tropomyosin compound "activity," we used both a biochemical and cell biology approach. To ascertain whether there was a direct interaction of TR100 with the target protein Tm5NM1, we used purified proteins to assess the impact of TR100 on actin filament kinetics using a pyrene model of actin filament depolymerization. Kostyukova and Hitchcock (30) have previously shown tropomyosin to have a role in inhibiting F-actin depolymerization, a finding that can now be extended to Tm5NM1. In the presence of saturating amounts of Tm5NM1, F-actin depolymerization was reduced by approximately 40% over the time course measured (Supplementary Fig. S2A). Using this model, we investigated the impact of TR100 on actin filament dynamics. The difference in the rate of filament depolymerization (V_0) between F-actin and Tm5NM1-coated F-actin is negated by TR100 (Supplementary Fig. S2B and S2C). These data show a direct interaction between TR100 and Tm5NM1 resulting in enhanced actin filament depolymerization *in vitro*.

To confirm whether this impact on actin filament stability held true in a cell system, we assessed actin solubility in normal and transformed cells treated with TR100. Normal (MEFs) and transformed (neuroblastoma SH-EP) cells were treated with increasing concentrations of TR100 for 24 hours, and soluble (G) versus insoluble (F) actin was quantified using a G:F actin assay (Fig. 2E). Although we observed a shift in the solubility of actin upon treatment with TR100 in both the normal and transformed cells, the transformed SH-EP cells showed a more significant sensitivity to TR100 at both 5 and 7.5 μmol/L (Fig. 2F). This increase in actin filament solubility was also observed using immunofluorescence studies. MEFs and SH-EP cells were treated with increasing concentrations of TR100 for 24 hours, and total actin filament (Fig. 2G) or Tm5NM1/2 (Fig. 2H) organization was evaluated using the well-established microfilament disruption assay (31). Although there was a slight decrease in actin and Tm5NM1/2-containing filament staining in MEF cells treated with TR100 (Fig. 2G and H, top), TR100 treatment of the transformed SH-EP cells resulted in a significant disruption of both actin and Tm5NM1/2-containing filaments in a dose-dependent manner (Fig. 2G and H, bottom). Taken together, our data suggest that TR100 is more effective in disabling the actin cytoskeleton of transformed cells than normal cells.

TR100 selectively disrupts cytoskeletal Tm5NM1/2 containing actin filaments

Although treatment with TR100 severely impacted both the total actin organization (Fig. 2G) and the integrity of Tm5NM1/2-containing filaments (Fig. 2H), no significant impact on the organization of the microtubules was observed suggesting that this compound preferentially targeted the actin microfilaments (Supplementary Fig. S3).

To determine whether TR100 was able to show isoform specificity, the integrity of the endogenous tropomyosin-containing filaments was assessed. MEF cells treated with

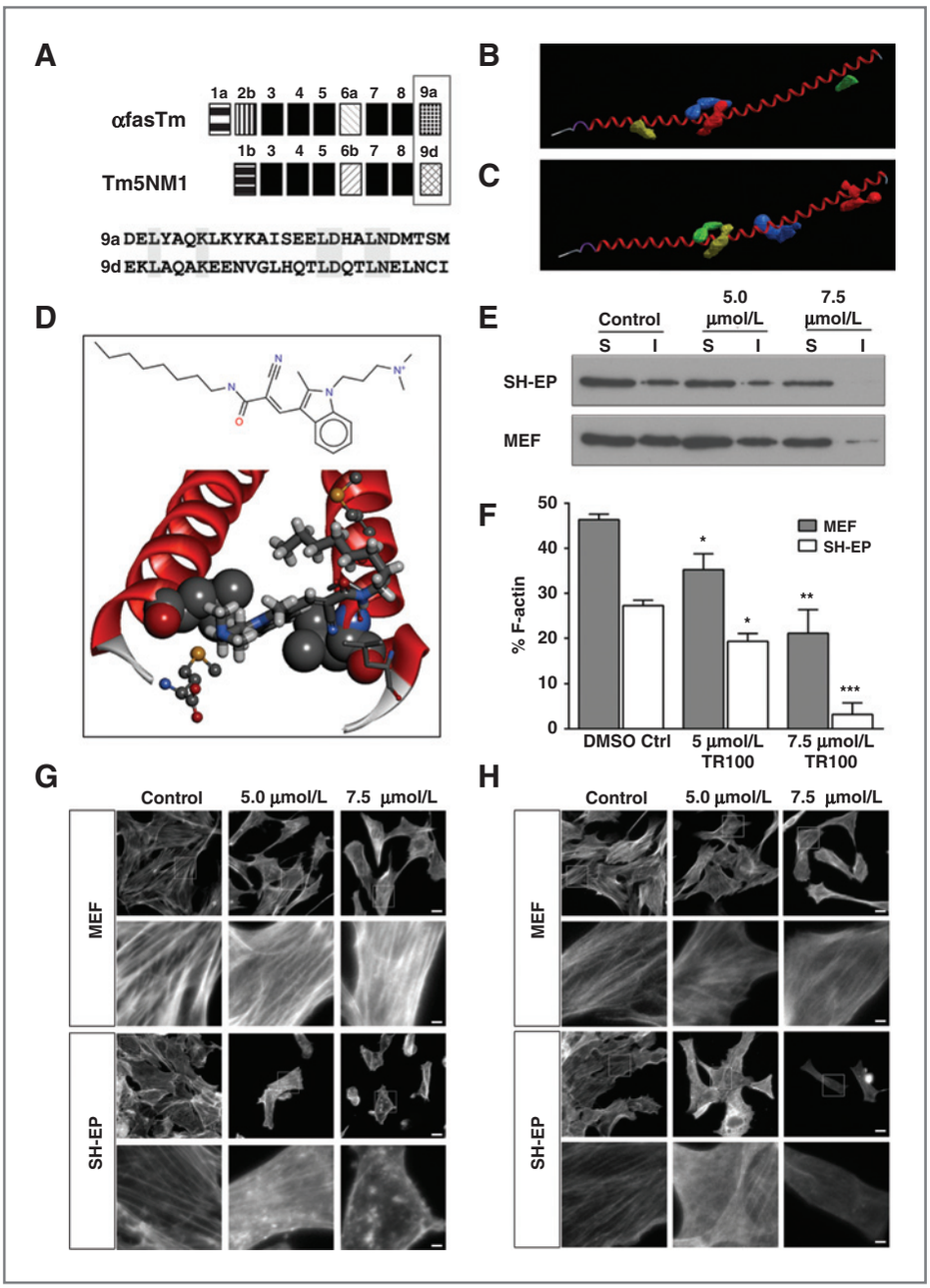

Figure 2. Lead anti-tropomyosin compound TR100 disrupts the actin cytoskeleton. A, tropomyosin splice variant alignment of cytoskeletal Tm5NM1/2 and muscle αTmfast tropomyosin highlighting the sequence divergence of the isoforms. Homology modeling was conducted and potential compound-binding pockets were identified using Molsoft ICM's pocket finder. B and C, shown are single α helices of αTmfast tropomyosin (B) and Tm5NM1 (C) with the binding pockets labeled in arbitrary colors. D, the structure of TR100 and modeling of predicted interaction of TR100 with the C-terminus (9d exon) of Tm5NM1. E, Western blot analysis of the G:F actin assay showing soluble (S) and insoluble (I) actin from MEF and SH-EP cells treated with increasing concentrations (0, 5, and 7.5 µmol/L) of TR100. F, quantitation of % F-actin from G:F actin assay. MEF and SH-EP cells treated with increasing concentrations (0, 5, and 7.5 µmol/L) of TR100 for 24 hours and impact on the actin cytoskeleton was assessed using the microfilament disruption assay. G and H, cells were stained with phalloidin (G) to visualize the actin cytoskeleton or with γ\9d (H) to visualize Tm5NM1 containing actin filaments. Scale bar, 10 µm (2 µm inset). Data points in F represent the average of n = 3 ± SEM. *, $P < 0.05$; **, $P < 0.01$; ***, $P < 0.001$.

increasing doses (0, 0.1, 1, and 10 µmol/L) or for increasing time (10 µmol/L for 0, 1, 4, and 8 hours) with TR100 showed an initial preferential loss of LMW Tm5NM1/2-containing filaments compared with the HMW tropomyosins (Supplementary Fig. S4A–S4L). However, at higher dose and longer exposure times of TR100, we did observe an increase in the number of cells displaying no stress fibers (Supplementary Fig. S4M, S4N, and S4I–S4L). Although the cytoskeletal tropomyosins differ in the amino terminus exon choice, all contain the carboxyl terminal exon 9d. Therefore, this lack of absolute specificity of TR100 is most likely due to the high degree of sequence similarity between the 9d exon of the different tropomyosin genes (9).

From a clinical perspective, it may not be critical that the anti-tropomyosin compounds discriminate between HMW and LMW cytoskeletal tropomyosins. It is essential, however, that these compounds are able to discriminate between the actin filaments involved in tumor cell progression and those that are crucial for sarcomeric integrity and contractile function. Cytoskeletal and muscle tropomyosins differ at the C-terminus due to alternative splicing of exon 9 (Fig. 2A). Live cell imaging analysis was conducted on NIH3T3 fibroblast cells, which stably expressed either the cytoskeletal mCherry-Tm5NM1 or the muscle YFP-αTmfast. Cells were treated with 2 µmol/L TR100 and imaged for 24 hours. Representative

images at 0, 15, 19, and 24 hours are shown (Fig. 3A). Cells expressing the cytoskeletal Tm5NM1 were more sensitive to TR100 treatment as measured by a marked reduction at 24 hours in actin filament organization compared with cells expressing the muscle αTmfast (Fig. 3A). To determine whether TR100 could discriminate between the 9a and 9d terminus, MEFs were transiently transfected with constructs expressing either a fluorescently-tagged Tm5NM1 (exon 9d) or Tm5NM5, a modified Tm5NM1 containing the C-terminus of muscle Tm (exon 9a). MEFs overexpressing the Tm5NM1 (9d) were significantly more sensitive to TR100 than cells overexpressing Tm5NM5 (9a; Fig. 3B and C), both in terms of filament stability and cell size. These initial experiments show that it is possible to discriminate between cytoskeletal and muscle actin filament populations and target distinct actin filaments based on the tropomyosin composition.

TR100 has minimal impact on differentiated cells

The expression of Tm5NM1/2 was undetectable in isolated rat ACMs (Fig. 4A); therefore, we predicted that TR100 would have minimal impact on the contractile function of an ACM. Cardiotoxic effects of TR100 were assessed using a specialized IonOptix Corp system, which is routinely used to measure real-time changes in sarcomere shortening of a contracting isolated rat ACM (27, 32). Shown are representative contraction curves (Fig. 4B). Alterations in peak shortening of the ACM sarcomere was used to assess changes in contractile function in the presence and absence of TR100 and a known cytoskeleton disrupting agent cytochalasin D.

To establish an effective TR100 concentration for the functional experiments, live imaging analysis was conducted on SKN-Be2C neuroblastoma cells in parallel with ACMs. TR100 at 10 μmol/L had a profound impact on both SKN-Be2C cell

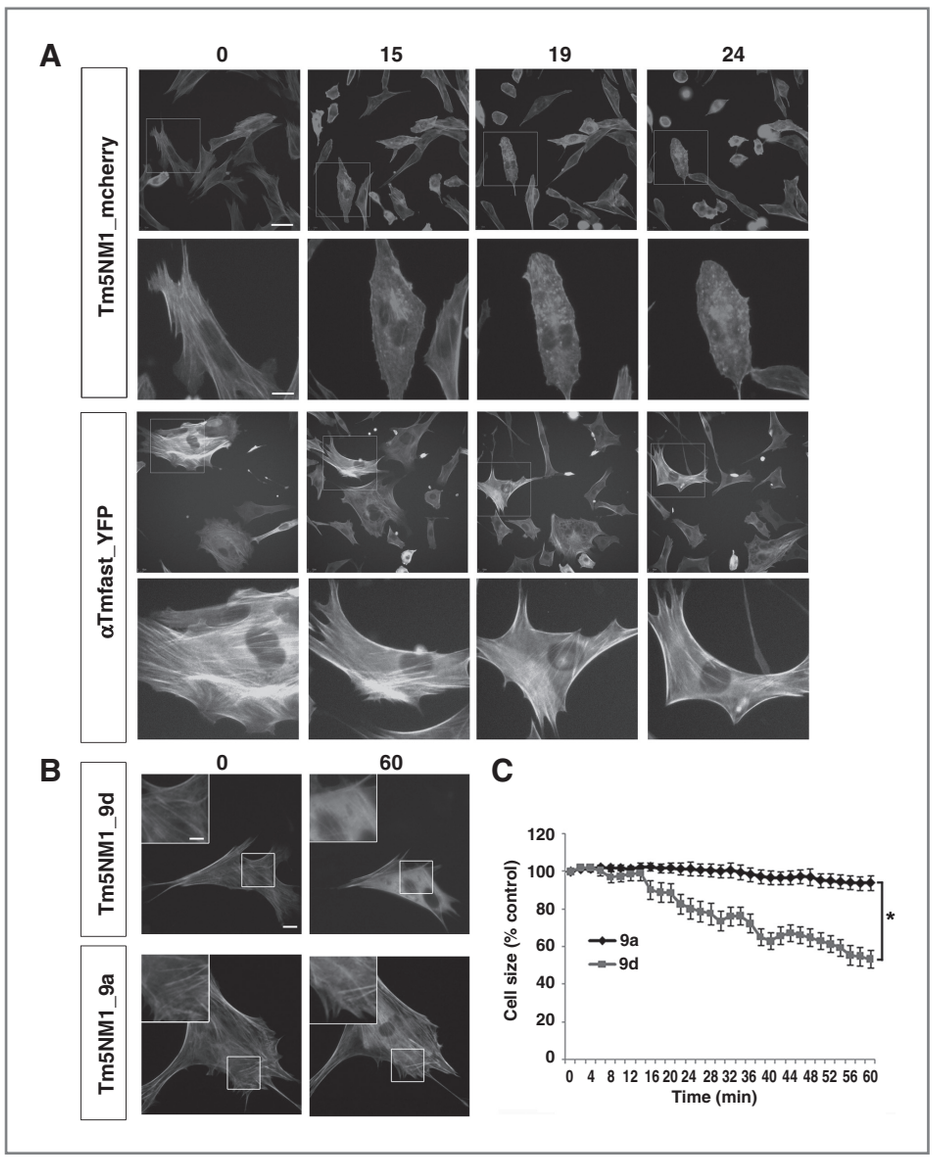

Figure 3. TR100 preferentially targets cytoskeletal Tm5NM1-containing filaments. A, NIH3T3 cells overexpressing Tm5NM1 tagged with mCherry or αfastTm tagged with YFP were treated with 2 μmol/L TR100 and imaged every 5 minutes for 24 hours. Representative images at 0, 15, 19, and 24 hours following drug treatment. B, images of MEFs transiently transfected with fluorescently tagged Tm5NM1 (9d) or Tm5NM5 (9a) were treated with TR100 (10 μmol/L) and imaged every 2 minutes for 60 minutes. C, change in cell size is measured as a percentage of 0 minute control. Data points in C represent $n = 10$ cells from 3 independent experiments. Scale bar, 20 μm (10 μm insets). *, $P < 0.05$.

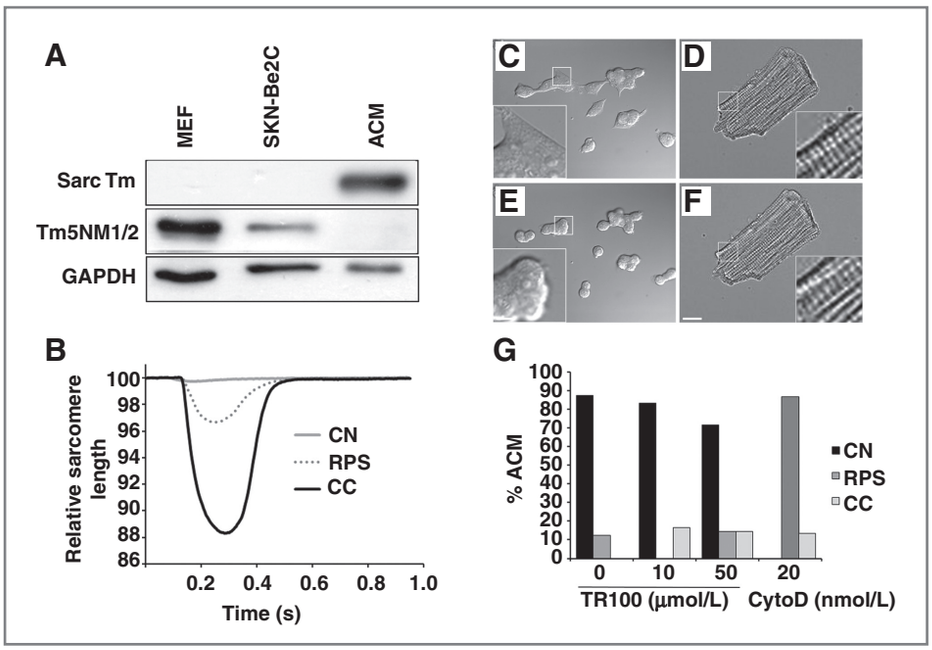

Figure 4. TR100 has minimal impact on the contractile function of isolated rat cardiomyocytes. A, Western blot analysis of expression levels of sarcomeric tropomyosin (top) and LMW cytoskeletal Tm5NM1/2 (middle) in MEFs, neuroblastoma (SKN-Be2C) cells, and ACMs. B, representative contraction curves of ACMs showing normal peak shortening (contracted normally CN, black), reduced peak shortening (RPS, gray dotted), and ceased contraction (CC, gray). C, live imaging analysis (0 and 6 minutes) of SKN-Be2C (C and E) and ACM (D and F) treated with 10 μmol/L of TR100 (E and F). Scale bar, 20 μm (5 μm insets). G, histograms of % cells, which contracted normally (CN, black bars), showed reduced peak shortening (RPS, dark gray bars) or ceased contraction (CC, light gray bars) in the presence of TR100 or actin-targeting drug cytochalasin D (CytoD). Graph points represent the pooled data of 14 individual ACMs isolated from $n = 3$ animals. GAPDH, glyceraldehyde-3-phosphate dehydrogenase.

adherence and viability as early as 6 minutes posttreatment (Fig. 4C and E). In contrast, ACMs seemed to be structurally intact (Fig. 4D and F). In functional studies, ACMs perfused with 10 μmol/L TR100 for 6 minutes showed little to no change in the contractile properties, which is represented by 87% of the cells contracting normally (Fig. 4G). High-dose exposure of 50 μmol/L TR100 revealed toxicity in ACMs that was displayed as reduced peak shortening (14%) and cessation of contraction (14%; RPS and CC, respectively; Fig. 4G). In contrast, more than 87% of ACMs exposed to the ubiquitous actin destabilizing drug cytochalasin D showed a profound decrease in contractile shortening. TR100, unlike other actin-targeting compounds such as cytochalasin D, does not acutely impact the contractile function of isolated ACMs. This shows that it is possible to develop anti-tropomyosin compounds, which can discriminate between the cytoskeleton and the contractile apparatus of cardiac muscle.

Because Tm5NM1/2 is also required for neuronal function (33), neurotoxicity is a potential side effect of TR100. To determine the effect of TR100 on neuronal integrity, long-term cultures of terminally differentiated hippocampal neurons were incubated with increasing concentrations of TR100 and the synapses visualized by staining for synaptophysin (presynaptic), F-actin (using phalloidin, postsynaptic), and DAPI to visualize the nucleus (Supplementary Fig. S5A and S5B). TR100, at a dose that was effective against SKN-Be2C tumor cells, had no overt effect on neuronal cell viability as determined by the integrity of their nuclei and the presence of neuronal synapses (Supplementary Fig. S5C). This result raises the possibility that TR100 may impact dividing cells at doses that have minimal impact on terminally differentiated cells such as ACMs and hippocampal neurons.

TR100 is effective in 2D and 3D tumor cell cultures

A representative transformed melanoma cell line (SK-MEL-28; Fig. 5A–D) and a primary human melanocyte cell line (Fig. 5E–H) were treated with either DMSO (Fig. 5A, C, E, and G) or 5 μmol/L TR100 (Fig. 5B, D, F, and H) and Tm5NM1/2-containing filament organization evaluated using a microfilament disruption assay. As observed with the MEF and SH-EP comparison (Fig. 2E–H), TR100 had a more significant impact on actin filament integrity in the transformed SK-MEL-28 melanoma cells than the primary human melanocytes (Fig. 5C vs. D, G vs. H, respectively). This correlated with differences in sensitivity of these cell lines to TR100 in cytotoxicity assays (Fig. 5I), suggesting a strong correlation between Tm5NM1/2 filament disruption and efficacy. The calculated EC_{50} values for TR100 against SK-MEL-28 and melanocytes cell lines were 1.9 $\pm$ 0.08 μmol/L and 4.1 $\pm$ 0.07 μmol/L, respectively. In addition to the shift in EC_{50}, we also observed a significant difference in the maximal response in both these cell lines. TR100 had a reduced "killing effect" on the melanocytes with approximately 40% of cells remaining viable at the highest concentration of TR100 compared with approximately 0% with the transformed SK-MEL-28 cells (Fig. 5I). This change in maximal response is likely to mask any significant changes in the relative EC_{50} as

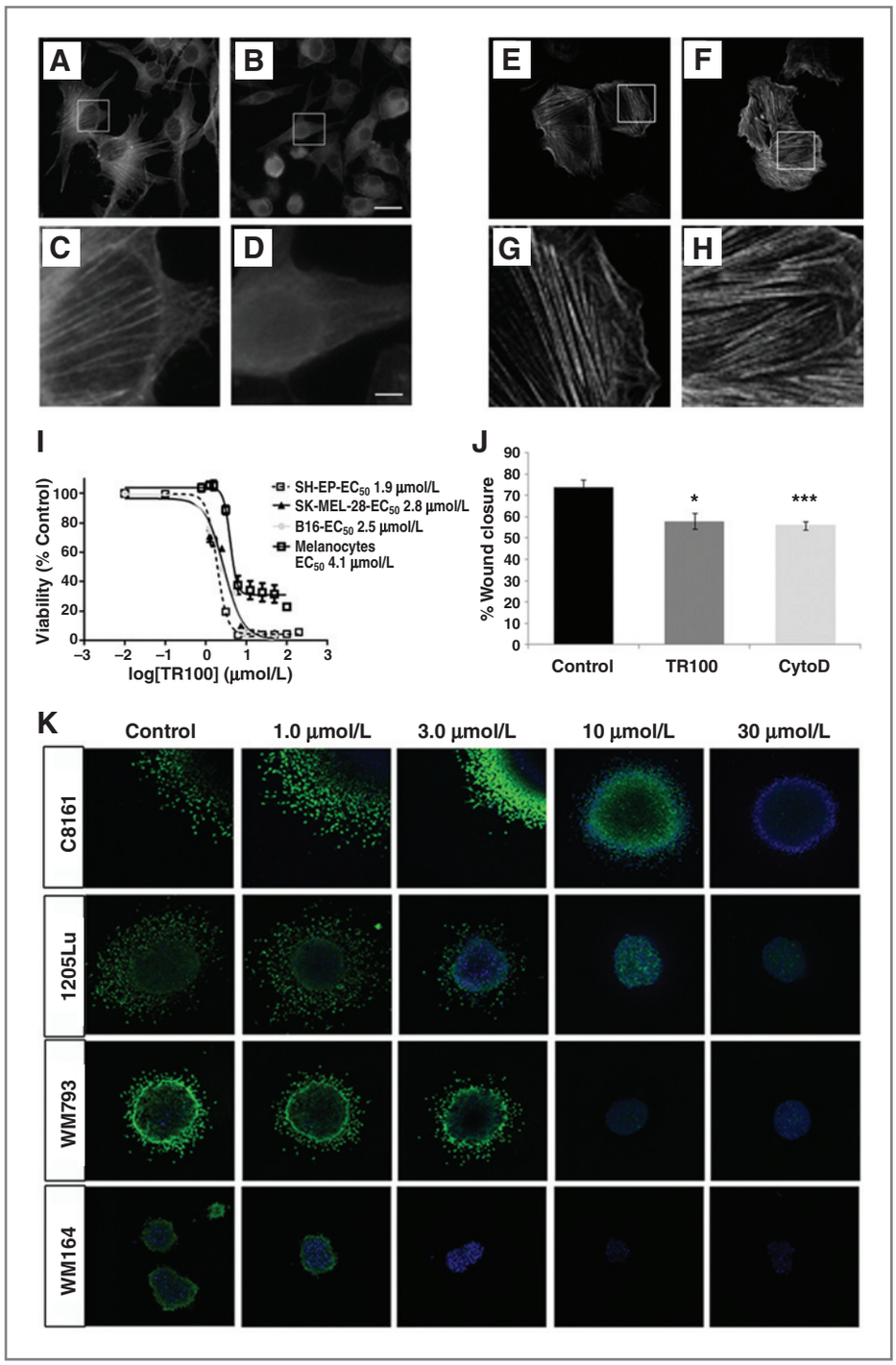

Figure 5. TR100 impacts tumor cell viability and motility in 2D and 3D cultures. Representative images of transformed melanoma SK-MEL-28 cells (A–D) and primary human melanocytes (E–H) untreated (A,C and E,G) or treated with 2 μmol/L TR100 (B,D and F,H) for 24 hours and Tm5NM1/2 filaments stained with γ\9d antibody. I, cytotoxicity curves in adherent (2D) cultures of representative neuroblastoma (SH-EP), melanoma (SK-MEL-28 and B16/F10), and melanocyte cell lines treated with TR100. J, SH-EP cells were treated with sublethal concentrations of TR100 (2.5 μmol/L) or cytochalasin D (cytoD; 20 nmol/L) and percent wound closure measured at 15 hour. K, 3D spheroid cultures of human melanoma cell lines derived from primary (WM793), lymph node metastatic (WM164), and distant metastatic (C8161 and 1205Lu) disease. Cells were cultured in nonadherent conditions for 72 hours, then transferred to a collagen matrix before being treated with DMSO or increasing concentrations of TR100. Cells were stained with calcein-AM and DAPI to visualize viable and nonviable cells, respectively. Data shown for each assay are representative of $n = 3$ independent experiments. *, $P < 0.05$; ***, $P < 0.001$. Scale bar, 20 μm (insets, 2 μm).

this represents the "effective concentration that provokes a response halfway between the minimum and maximum responses." TR100 was also efficacious against a panel of neural crest derived and pediatric tumor cell lines with an average EC_{50} 2.8 ± 0.3 μmol/L (Supplementary Table S1).

In addition, TR100 was tested in a 3D melanoma spheroid model (Fig. 5K). 3D spheroids implanted into a collagen gel matrix more accurately mimic tumor architecture and microenvironment (24, 25) and can be used for investigating the effects of small-molecule inhibitors on the growth and invasion of melanoma cells (34–36). Melanoma cell lines used in these assays were WM793, 1205Lu, and C8161, which display an invasive phenotype and WM164 a proliferative phenotype (37). At 3 μmol/L TR100, there was a significant impact on tumor

cell motility in spheroids grown from C8161 and 1205Lu cells (both derived from distant metastases) as shown by a decrease in live cells invading the collagen matrix. The WM164 cell line showed only little invasion, which was also inhibited at 3 μmol/L TR100. Interestingly, the effect on invasion was less on spheroids derived from the primary melanoma cell line WM793. At 10 μmol/L and 30 μmol/L TR100, we saw a marked increase in tumor cell death in spheroids of all melanoma cell lines, regardless of their stage or phenotype, as shown by an increase in cells staining positively for DAPI (Fig. 5K). In wound-healing assays, we were also able to show that TR100, at sublethal concentrations, significantly impacted wound closure in SH-EP neuroblastoma cells (Fig. 5J). This was a similar effect to what was observed with the actin-targeting drug cytochalasin D. This shows that disruption of the actin cytoskeleton with TR100 impacts both tumor cell motility and viability in melanoma and neuroblastoma cells.

TR100 induces apoptosis

Cell-cycle analysis of SK-MEL-28 cells treated with TR100 resulted in a significant increase in the sub G_1 or dead cell population (Supplementary Fig. S6A and S6B). This sub G_1 population significantly increased with exposure to 10 μmol/L TR100. This also correlated with an increase in levels of cleaved PARP (Supplementary Fig. S6C), a downstream target of the executioner caspase, caspase-3, which is activated during programmed cell death (38). We also observed a time-dependent increase in mitochondrial membrane permeability in SK-MEL-28 cells treated with TR100 as measured by a decrease in TMRE perchlorate fluorescence (Supplementary Fig. S6D). These data suggest that TR100 induces cell death most likely through the mitochondrial apoptotic pathway.

TR100 inhibits tumor growth in melanoma and neuroblastoma models

The efficacy of TR100 was assessed *in vivo* using 3 animal models: The B16/F10 murine melanoma model, the 1205Lu metastatic human melanoma xenograft model, and the CHP134 neuroblastoma xenograft model. In pilot experiments, the maximum-tolerated dose (MTD) of TR100 was determined for each genetic background of the mouse strains used for the tumor experiments. MTDs were 30 mg/kg^{-1} for C57BL/6 mice, 25 mg/kg^{-1} for BALB/c mice, and 20 mg/kg^{-1} for NOD/SCID mice. The dose of TR100 administered was selected on the basis of the dose that showed minimal adverse effects (data not shown). Treatment with TR100 resulted in a significant reduction in tumor growth (mm^3) compared with the vehicle control in all 3 models (Fig. 6A–C). On termination of the B16/F10 experiment, tumors from control ($n = 6$) and 30 mg/kg^{-1} ($n = 4$) TR100-treated animals were harvested and profiled for tropomyosin expression. We observed a significant decrease in the levels of Tm5NM1/2 in the 30 mg/kg^{-1} treated animals compared with the control-treated group with no detectable changes to the expression profile of the HMW Tm2 (Fig. 6D), suggesting that long-term exposure to TR100 impacts the expression level of the target Tm5NM1/2.

TR100 does not compromise the liver or heart *in vivo*

Targeting the actin cytoskeleton has the potential to cause both liver (39) and cardiac toxicity (40). Bloods were harvested from control and TR100-treated 1205Lu mouse xenograft model. TR100 treatment resulted in no changes in the levels of liver damage biomarkers ALP, AST, and ALT (Supplementary Fig. S7A) or the level of total bilirubin (Supplementary Fig. S7B). These data indicate that TR100 does not impact liver function. Manipulation of tropomyosin isoform contribution to the heart may result in compensatory hypertrophy of the cardiac muscle (40). Hearts were harvested from control and TR100-treated B16/F10 animals, and the structural integrity of the cardiac muscle was analyzed. Animals treated with TR100 showed no evidence of increased fibrosis in Massons Trichrome stained sections (Fig. 7A) or acute cardiomyocyte damage as measured by circulating blood troponin I levels (Fig. 7B). There were no overt signs of hypertrophy as measured by IVS (Fig. 7A and C) or changes in heart weight (Fig. 7D). TR100 is therefore able to inhibit tumor growth at doses that do not compromise the heart.

Discussion

Tropomyosin is an important regulator of the actin cytoskeleton (9, 41) and a key component of the actin microfilaments in tumor cells (1, 42). In this study, we have shown that tropomyosin is necessary to provide the cytoskeletal structure required for tumor cell survival. This finding is in accordance with the studies investigating tropomyosin knockout mouse models. Single knockout of the *TPM1* (43), *TPM2* (44), or *TPM3* (45) gene resulted in embryonic lethality, suggesting that at least 3 of the tropomyosin genes are providing nonredundant functions essential for embryo development. A question now being addressed by many research groups is what is the functional role of specific tropomyosin isoforms? Studies done by Tojkander and colleagues showed that knockdown of different single isoforms of tropomyosin can inhibit stress fiber formation in osteosarcoma cells, indicating that each isoform contributes a specific functional capacity (13). There is also increasing evidence in the literature to suggest that tropomyosins define functionally distinct actin filaments by regulating the recruitment and association of actin-binding proteins in an isoform-specific manner (13–15, 46, 47). This functional and spatial regulation of actin filaments has been shown to be conserved from yeast (14, 15) to mammals (12, 46) and provides a unique opportunity to target distinct actin filaments based on the tropomyosin composition. In this study, we designed anti-tropomyosin compounds that targeted the cytoskeletal tropomyosins, in particular, LMW Tm5NM1/2. These Tm5NM1-containing filaments were attractive targets in terms of disabling the filaments involved in tumor cell survival.

Understanding the mechanism by which these anti-tropomyosin compounds initiate tumor cell death is necessary for therapeutic application. The actin cytoskeleton is believed to have a role as both an initiator of apoptosis due to its role in the maintenance of cellular integrity and also as an integral component of the morphologic changes, which are a hallmark

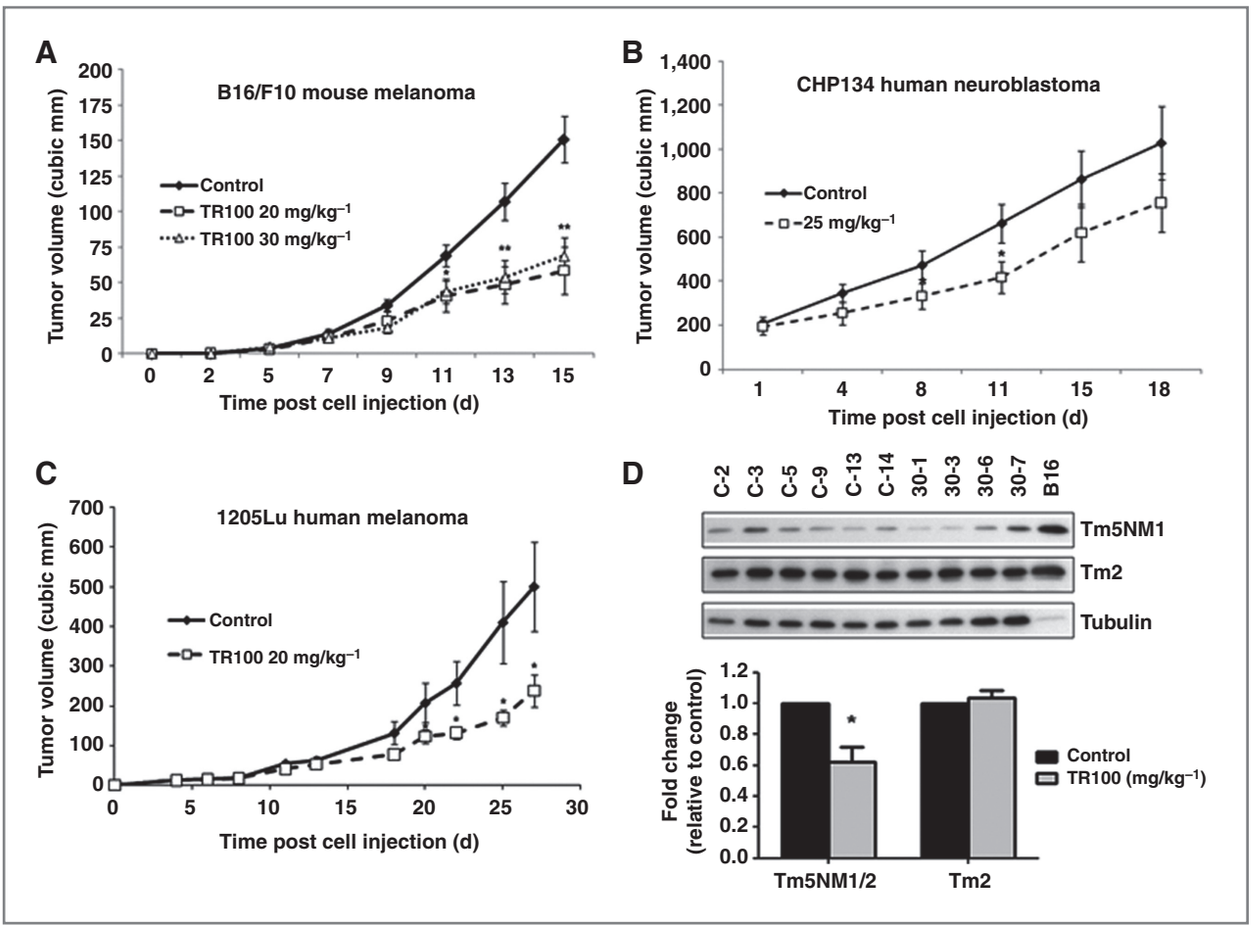

Figure 6. TR100 inhibits tumor growth in melanoma and neuroblastoma mouse models. A, B16/F10 mouse melanoma model: C57/BL6 animals were injected with B16/F10 cells and $n = 15$ per group were treated with DMSO, 20 mg/kg^{-1} or 30 mg/kg^{-1} of TR100 for 5 days/week for 2 weeks. Graph points represent an average of $n \geq 12$ animals per group $\pm$ SEM. For statistical analysis, control animals were compared with both 20 mg/kg^{-1} and 30 mg/kg^{-1} at day 9, 11, and 15. B, CHP134 human neuroblastoma xenograft model: athymic nude mice (nu$^-$/nu$^-$) animals were injected with CHP134 cells and $n = 9$ animals per group were treated with 10% (v/v) DMSO in PBS (control) or 25 mg/kg^{-1} of TR100 each day for 3 weeks. Graph points represent an average of $n \geq 7$ animals per group $\pm$ SEM. For statistical analysis, control animals were compared with 25 mg/kg^{-1} TR100 at day 4, 8, 11, 15, and 18. *, $P < 0.05$; **, $P < 0.01$. C, 1205Lu human melanoma model: nonobese diabetic/severe combined immunodeficient (NOD/SCID) animals were injected with 1205Lu cells and $n = 10$ animals per group were treated with DMSO (control) or 20 mg/kg^{-1} of TR100 each day for 4 weeks. Graph points represent an average of $n \geq 8$ animals per group $\pm$ SEM. For statistical analysis, control animals were compared with 20 mg/kg^{-1} TR100 at day 20, 22, 25, and 27. D, tumors from control ($n = 6$) and 30 mg/kg^{-1} ($n = 4$) treated animals were harvested and levels of LMW cytoskeletal Tm5NM1/2 (top) and HMW cytoskeletal Tm2 (middle) were analyzed and quantitated [DMSO control (black bars) and 30 mg/kg^{-1} (gray bars)]. *, $P < 0.05$.

of apoptosis (48). Actin-targeting drugs such as the cytochalasins or jasplakinolide have been widely used to induce apoptosis in a variety of cell types (49) for many years, yet the role actin has in controlling the initiation of apoptosis is only now becoming apparent. Studies have shown that manipulating the G-F actin ratio can trigger apoptosis, but this seems to be largely dependent on cell type (50). Previous studies have shown that altering the level of tropomyosin impacts actin polymer accumulation (51) and F-actin solubility (52). One possibility is the anti-tropomyosin compounds, by altering the associated tropomyosin, are changing the G-F actin ratio and thereby triggering cell death. Alternatively, Puthalakath and colleagues showed that both the treatment of cells with cytochalasin D and induction of anoikis caused the liberation of Bmf, a BH3-only pro-apoptotic protein that is sequestered to the actin cytoskeleton (53). Therefore, disrupting the actin cytoskeleton with the anti-tropomyosin compounds may result in the dissociation of Bmf and the initiation of cell death via the mitochondrial apoptotic pathway. Although we know that the anti-tropomyosin compounds initiate cell death, the exact mechanism is still being elucidated.

Tropomyosins are widely expressed in many cell types of the body. Knockout of just Tm5NM1/2 leads to 50% embryonic lethality (with respect to 100% for the whole *TPM3* gene) in multiple mouse backgrounds indicating that it is required for normal embryonic development (54). Nevertheless, if knockout animals survive embryogenesis they have a normal lifespan and display no cardiac phenotype (54). In this study, we have also shown that the anti-tropomyosin compound, TR100, did not impact differentiated cells. Taken together, this suggests

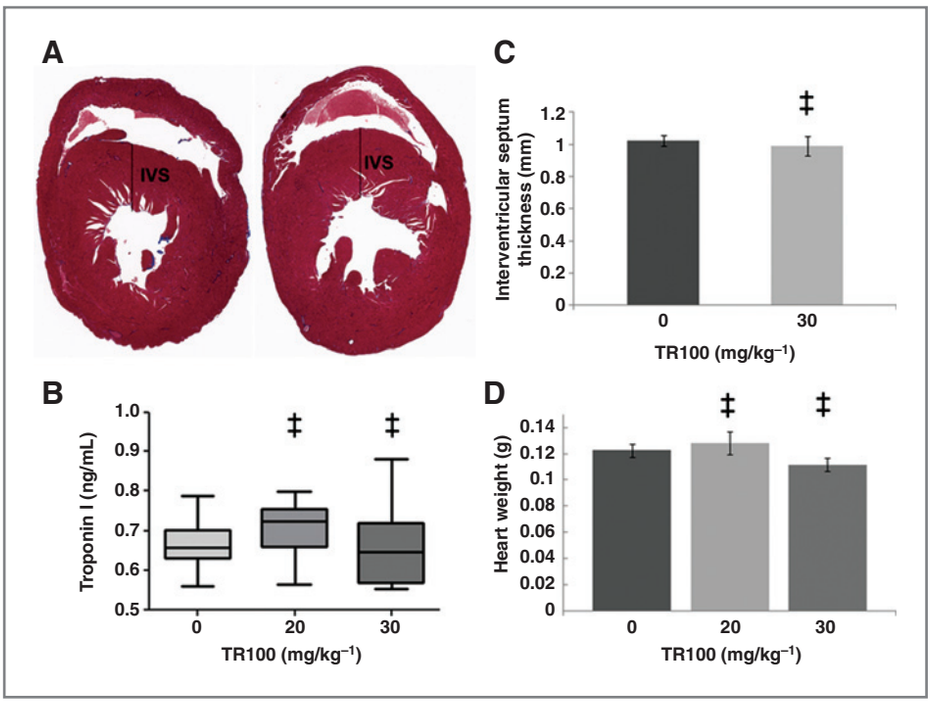

Figure 7. TR100 shows minimal cardiotoxicity *in vivo*. A, transverse sections of the heart from control and 30 mg/kg^{-1} TR100-treated B16/F10 xenotransplant animals stained with Massons Trichrome to assess for necrosis/fibrosis. B, circulating troponin I levels measured from control, 20 mg/kg^{-1} and 30 mg/kg^{-1} TR100-treated groups using a cTnI Elisa. Cardiac hypertrophy IVS (representative measurement shown in A) was measured in control and 30 mg/kg^{-1} TR100-treated mice (C) and hearts weighed post cull for control, 20 mg/kg^{-1} and 30 mg/kg^{-1} TR100-treated animals (D). Box plots in B are the average of $n \geq 8$ animals per group ± SEM. Graphs C and D are the average of $n \geq 12$ animals per group ± SEM. ‡, not significant.

that targeting of just Tm5NM1/2 would be unlikely to have toxicity to any extent approaching that of anti-actin drugs. The first-in-class anti-tropomyosin compounds we studied do target a range of cytoskeletal tropomyosins with an evolutionarily conserved C-terminus, which may account for the toxicity observed in the MTD studies. We are currently refining the drug design to achieve greater isoform specificity. This novel approach and the development of the new class of anti-tropomyosin compounds may be the key for disabling a long sought after target, the actin cytoskeleton. Development of such agents holds enormous implications for the treatment of cancers beyond neuroblastoma and melanoma.

Disclosure of Potential Conflicts of Interest

J.R. Stehn has ownership interest (including patents) in Trobio Pty Ltd and is a consultant/advisory board member of Genscreen Pty Ltd. H. Treutlein is employed (other than primary affiliation; e.g., consulting) as a CEO in Computist Bio-Nanotech. I. Dixon is employed (other than primary affiliation; e.g., consulting) as director and shareholder, has commercial research grant, and has ownership interest (including patents) in Trobio Pty Ltd and Genscreen Pty Ltd. P.W. Gunning has commercial research support and ownership interest (including patents) in Trobio Pty Ltd. No potential conflicts of interest were disclosed by the other authors.

Authors' Contributions

Conception and design: J.R. Stehn, N.K. Haass, G. Kottyan, M. Allanson, T. Fath, A. McCluskey, T.P. Cripe, P.W. Gunning

Development of methodology: J.R. Stehn, N.K. Haass, T. Bonello, G. Kottyan, H. Treutlein, T.L. Butler, T.A. Hill, D. Winlaw, V.E. Reeve, T.P. Cripe, P.W. Gunning

Acquisition of data (provided animals, acquired and managed patients, provided facilities, etc.): J.R. Stehn, N.K. Haass, T. Bonello, M. Desouza, G. Kottyan, P.R. Nascimento, V.B. Sequeira, T.L. Butler, M. Allanson, T. Fath, S.J. Palmer, E.C. Hardeman, V.E. Reeve, T.P. Cripe, P.W. Gunning

Analysis and interpretation of data (e.g., statistical analysis, biostatistics, computational analysis): J.R. Stehn, N.K. Haass, T. Bonello, M. Desouza, G. Kottyan, H. Treutlein, J. Zeng, V.B. Sequeira, T.L. Butler, M. Allanson, T. Fath, S.J. Palmer, E.C. Hardeman, D. Winlaw, V.E. Reeve, W. Weninger, T.P. Cripe, P.W. Gunning

Writing, review, and/or revision of the manuscript: J.R. Stehn, N.K. Haass, T. Bonello, G. Kottyan, H. Treutlein, G. Schevzov, D. Winlaw, W. Weninger, T.P. Cripe, P.W. Gunning

Administrative, technical, or material support (i.e., reporting or organizing data, constructing databases): N.K. Haass, G. Kottyan, G. Schevzov, T. P. Cripe

Study supervision: J.R. Stehn, N.K. Haass, W. Weninger, T.P. Cripe, P.W. Gunning

Provision of inhibitors designed to inhibit tropomyosin for use in the experiments: I. Dixon

Acknowledgments

The authors thank M. Herlyn (The Wistar Institute, Philadelphia, PA) for providing the melanoma cell lines, R. Mason (University of Sydney) for providing the primary melanocyte cell lines, G. Tsoukalas and C. Gotsis (Veterinary Pathology Diagnostic Services, University of Sydney) for blood biochemistry analysis, Biomedical Imaging Facility, University of NSW, and the following people for technical assistance: B. Roediger, A. Nehme, L. Corcoran, M. Nguyen, A. Swain, N. Berents, M. Currier, D. Eaves, and E. Jousma.

Grant Support

This work was supported by generous donations from The Kids Cancer Project, (TKCP). Grants include: Project grant 1004188 from the Australian National Health and Medical Research Council (NHMRC) for P.W.G P.W. Gunning and J.R. Stehn, Project Grant RG 09-08 (Cancer Council New South Wales), N.K. Haass was supported by Project Grant 570778 (Priority-driven collaborative cancer research scheme/Cancer Australia/Cure Cancer Australia Foundation), Research Innovation Grant 08/RFG/1-27 (Cancer Institute New South Wales), and Project Grant 1003637 (NHMRC). D. Winlaw was supported by a National Heart Foundation of Australia Career Development Grant. W. Weninger was supported by grants from the NHMRC and the NSW government. J.R. Stehn is a TKCP C4 Research Fellow. N.K. Haass is a recipient of the Cameron Fellowship from the Melanoma and Skin Cancer Research Institute, Australia. T. Bonello is a recipient of a Cancer Institute of NSW Research Scholar award. M. Desouza is recipient of a Translational Cancer Research Network Scholar award.

The costs of publication of this article were defrayed in part by the payment of page charges. This article must therefore be hereby marked *advertisement* in accordance with 18 U.S.C. Section 1734 solely to indicate this fact.

Received December 9, 2012; revised April 10, 2013; accepted May 17, 2013; published online August 14, 2013.

References

1. Helfman DM, Flynn P, Khan P, Saeed A. Tropomyosin as a regulator of cancer cell transformation. Adv Exp Med Biol 2008;644:124–31.
2. Hall A. The cytoskeleton and cancer. Cancer Metastasis Rev 2009;28:5–14.
3. Rao J, Li N. Microfilament actin remodeling as a potential target for cancer drug development. Curr Cancer Drug Targets 2004;4:345–54.
4. Yamaguchi H, Condeelis J. Regulation of the actin cytoskeleton in cancer cell migration and invasion. Biochim Biophys Acta 2007; 1773:642–52.
5. Bonello TT, Stehn JR, Gunning PW. New approaches to targeting the actin cytoskeleton for chemotherapy. Future Med Chem 2009;1: 1311–31.
6. Bousquet PF, Paulsen LA, Fondy C, Lipski KM, Loucy KJ, Fondy TP. Effects of cytochalasin B in culture and *in vivo* on murine Madison 109 lung carcinoma and on B16 melanoma. Cancer Res 1990;50: 1431–9.
7. Senderowicz AM, Kaur G, Sainz E, Laing C, Inman WD, Rodriguez J, et al. Jasplakinolide's inhibition of the growth of prostate carcinoma cells *in vitro* with disruption of the actin cytoskeleton. J Natl Cancer Inst 1995;87:46–51.
8. Newman DJ, Cragg GM. Marine natural products and related compounds in clinical and advanced preclinical trials. J Nat Prod 2004; 67:1216–38.
9. Gunning P, O'Neill G, Hardeman E. Tropomyosin-based regulation of the actin cytoskeleton in time and space. Physiol Rev 2008;88:1–35.
10. Li XE, Holmes KC, Lehman W, Jung H, Fischer S. The shape and flexibility of tropomyosin coiled coils: implications for Aatin filament assembly and regulation. J Mol Biol 2009;395:327–39.
11. Gunning PW, Schevzov G, Kee AJ, Hardeman EC. Tropomyosin isoforms: divining rods for actin cytoskeleton function. Trends Cell Biol 2005;15:333–41.
12. Bryce NS, Schevzov G, Ferguson V, Percival JM, Lin JJ, Matsumura F, et al. Specification of actin filament function and molecular composition by tropomyosin isoforms. Mol Biol Cell 2003;14:1002–16.
13. Tojkander S, Gateva G, Schevzov G, Hotulainen P, Naumanen P, Martin C, et al. A molecular pathway for myosin II recruitment to stress fibers. Curr Biol 2011;21:539–50.
14. Coulton AT, East DA, Galinska-Rakoczy A, Lehman W, Mulvihill DP. The recruitment of acetylated and unacetylated tropomyosin to distinct actin polymers permits the discrete regulation of specific myosins in fission yeast. J Cell Sci 2010;123:3235–43.
15. Clayton JE, Sammons MR, Stark BC, Hodges AR, Lord M. Differential regulation of unconventional fission yeast myosins via the actin track. Curr Biol 2010;20:1423–31.
16. Stehn JR, Schevzov G, O'Neill GM, Gunning PW. Specialisation of the tropomyosin composition of actin filaments provides new potential targets for chemotherapy. Curr Cancer Drug Tar 2006;6:245–56.
17. Schevzov G, Vrhovski B, Bryce NS, Elmir S, Qiu MR, O'Neill GM, et al. Tissue-specific tropomyosin isoform composition. J Histochem Cytochem 2005;53:557–70.
18. Gordon-Thomson C, Jones J, Mason RS, Moore GP. ErbB receptors mediate both migratory and proliferative activities in human melanocytes and melanoma cells. Melanoma Res 2005;15:21–8.
19. Smalley KS, Brafford P, Haass NK, Brandner JM, Brown E, Herlyn M. Up-regulated expression of zonula occludens protein-1 in human melanoma associates with N-cadherin and contributes to invasion and adhesion. Am J Pathol 2005;166:1541–54.
20. Smalley KS, Contractor R, Haass NK, Lee JT, Nathanson KL, Medina CA, et al. Ki67 expression levels are a better marker of reduced melanoma growth following MEK inhibitor treatment than phospho-ERK levels. Br J Cancer 2007;96:445–9.
21. Creed SJ, Bryce N, Naumanen P, Weinberger R, Lappalainen P, Stehn J, et al. Tropomyosin isoforms define distinct microfilament populations with different drug susceptibility. Euro J Cell Biol 2008;87: 709–20.
22. Bach CT, Creed S, Zhong J, Mahmassani M, Schevzov G, Stehn J, et al. Tropomyosin isoform expression regulates the transition of adhesions to determine cell speed and direction. Mol Cell Biol 2009; 29:1506–14.
23. Gan PP, Pasquier E, Kavallaris M. Class III beta-tubulin mediates sensitivity to chemotherapeutic drugs in non small cell lung cancer. Cancer Res 2007;67:9356–63.
24. Smalley KS, Haass NK, Brafford PA, Lioni M, Flaherty KT, Herlyn M. Multiple signaling pathways must be targeted to overcome drug resistance in cell lines derived from melanoma metastases. Mol Cancer Ther 2006;5:1136–44.
25. Smalley KS, Lioni M, Noma K, Haass NK, Herlyn M. *In vitro* 3D tumor microenvironment models for anti-cancer drug discovery. Expert Opin Drug Discov 2008;3:1–10.
26. Fath T, Ke YD, Gunning P, Gotz J, Ittner LM. Primary support cultures of hippocampal and substantia nigra neurons. Nat Protoc 2009;4:78–85.
27. Butler TL, Egan JR, Graf FG, Au CG, McMahon AC, North KN, et al. Dysfunction induced by ischemia versus edema: does edema matter? J Thorac Cardiovasc Surg 2009;138:141–7.
28. Hahn WC, Counter CM, Lundberg AS, Beijersbergen RL, Brooks MW, Weinberg RA. Creation of human tumour cells with defined genetic elements. Nature 1999;400:464–8.
29. Thiele CJ. Neuroblastoma cell lines. In: Masters J editor. Human Cell Culture. Lancaster, UK: Kluwer Academic Publishers; 1998, Vol 1. p. 21–53.
30. Kostyukova A, Hitchcock-DeGregori SE. Effect of structure of the N terminus of tropomyosin on tropomodulin function. J Biol Chem 2004;279:5066–71.
31. Watts KR, Morinaka BI, Amagata T, Robinson SJ, Tenney K, Bray WM, et al. Biostructural features of additional jasplakinolide (jaspamide) analogues. J Nat Prod 2011;74:341–51.
32. Ren J. Attenuated cardiac contractile responsiveness to insulin-like growth factor I in ventricular myocytes from biobreeding spontaneous diabetic rats. Cardiovasc Res 2000;46:162–71.
33. Schevzov G, Bryce NS, Almonte-Baldonado R, Joya J, Lin JJ, Hardeman E, et al. Specific features of neuronal size and shape are regulated by tropomyosin isoforms. Mol Biol Cell 2005;16: 3425–37.
34. Haass NK, Sproesser K, Nguyen TK, Contractor R, Medina CA, Nathanson KL, et al. The mitogen-activated protein/extracellular signal-regulated kinase kinase inhibitor AZD6244 (ARRY-142886) induces growth arrest in melanoma cells and tumor regression when combined with docetaxel. Clin Cancer Res 2008;14:230–9.
35. Tsai J, Lee JT, Wang W, Zhang J, Cho H, Mamo S, et al. Discovery of a selective inhibitor of oncogenic B-Raf kinase with potent antimelanoma activity. Proc Natl Acad Sci U S A 2008;105:3041–6.
36. Lee JT, Li L, Brafford PA, van den Eijnden M, Halloran MB, Sproesser K, et al. PLX4032, a potent inhibitor of the B-Raf V600E oncogene, selectively inhibits V600E-positive melanomas. Pigment Cell Melanoma Res 2010;23:820–7.
37. Hoek KS, Eichhoff OM, Schlegel NC, Dobbeling U, Kobert N, Schaerer L, et al. *In vivo* switching of human melanoma cells between proliferative and invasive states. Cancer Res 2008;68:650–6.
38. Nicholson DW, Ali A, Thornberry NA, Vaillancourt JP, Ding CK, Gallant M, et al. Identification and inhibition of the ICE/CED-3 protease necessary for mammalian apoptosis. Nature 1995;376:37–43.
39. Herraez E, Macias RI, Vazquez-Tato J, Hierro C, Monte MJ, Marin JJ. Protective effect of bile acid derivatives in phalloidin-induced rat liver toxicity. Toxicol Appl Pharmacol 2009;239:21–8.
40. Wolska BM, Wieczorek DM. The role of tropomyosin in the regulation of myocardial contraction and relaxation. Pflugers Archiv 2003; 446:1–8.
41. O'Neill GM, Stehn JR, Gunning PW. Tropomyosins as interpreters of the signalling environment to regulate the local cytoskeleton. Semin Cancer Biol 2007;18:35–44.
42. Pawlak G, Helfman DM. Cytoskeletal changes in cell transformation and tumorigenesis. Curr Opin Genet Dev 2001;11:41–7.
43. Blanchard EM, Iizuka K, Christe M, Conner DA, Geisterfer-Lowrance A, Schoen FJ, et al. Targeted ablation of the murine alpha-tropomyosin gene. Circ Res 1997;81:1005–10.
44. Jagatheesan G, Rajan S, Wieczorek DF. Investigations into tropomyosin function using mouse models. J Mol Cell Cardiol 2010;48:893–8.

45. Hook J, Lemckert F, Qin H, Schevzov G, Gunning P. Gamma tropomyosin gene products are required for embryonic development. Mol Cell Biol 2004;24:2318–23.
46. McMichael BK, Kotadiya P, Singh T, Holliday LS, Lee BS. Tropomyosin isoforms localize to distinct microfilament populations in osteoclasts. Bone 2006;39:694–705.
47. Wawro B, Greenfield NJ, Wear MA, Cooper JA, Higgs HN, Hitchcock-DeGregori SE. Tropomyosin regulates elongation by formin at the fast-growing end of the actin filament. Biochemistry 2007;46:8146–55.
48. Kothakota S, Azuma T, Reinhard C, Klippel A, Tang J, Chu K, et al. Caspase-3-generated fragment of gelsolin: effector of morphological change in apoptosis. Science 1997;278:294–8.
49. Odaka C, Sanders ML, Crews P. Jasplakinolide induces apoptosis in various transformed cell lines by a caspase-3-like protease-dependent pathway. Clin Diagn Lab Immunol 2000;7:947–52.
50. Franklin-Tong VE, Gourlay CW. A role for actin in regulating apoptosis/programmed cell death: evidence spanning yeast, plants and animals. Biochem J 2008;413:389–404.
51. Schevzov G, Fath T, Vrhovski B, Vlahovich N, Rajan S, Hook J, et al. Divergent regulation of the sarcomere and the cytoskeleton. J Biol Chem 2008;283:275–83.
52. Creed SJ, Desouza M, Bamburg JR, Gunning P, Stehn J. Tropomyosin isoform 3 promotes the formation of filopodia by regulating the recruitment of actin-binding proteins to actin filaments. Exp Cell Res 2010;317:249–61.
53. Puthalakath H, Villunger A, O'Reilly LA, Beaumont JG, Coultas L, Cheney RE, et al. Bmf: a proapoptotic BH3-only protein regulated by interaction with the myosin V actin motor complex, activated by anoikis. Science 2001;293:1829–32.
54. Hook J, Lemckert F, Schevzov G, Fath T, Gunning P. Functional identity of the gamma tropomyosin gene: implications for embryonic development, reproduction and cell viability. Bioarchitecture 2011;1:49–59.